Catalysis Letters Vol. 103, Nos. 1–2, September 2005 (© 2005)
DOI: 10.1007/s10562-005-6498-2

An FT-IR study of NO_2 reduction in nanocrystalline NaY zeolite: effect of zeolite crystal size and adsorbed water

Gonghu Li, Sarah C. Larsen*, and Vicki H. Grassian*
Department of Chemistry, The University of Iowa, Iowa City, IA, 52242

Received 8 February 2005; accepted 9 May 2005

In this study, *in situ* transmission FT-IR spectroscopy was employed to investigate the selective catalytic reduction (SCR) of NO_2 in nanocrystalline NaY zeolite with a crystal size of 23 nm. Two specific aspects of this reaction were explored in this study: the importance of zeolite crystal size and the effect of water on the propylene-SCR reactions.

KEY WORDS: selective catalytic reduction; NO_2; zeolites; propylene; nanocrystals.

1. Introduction

Zeolites are widely used as catalysts because of their well defined three-dimensional pore structures, unique ion exchange capacity and acid–base properties [1]. For example, zeolite Y is the primary component in the industrial fluid catalytic cracking process [2]. Another important application of zeolites is emission abatement, such as in deNO_x catalysis [3]. Selective catalytic reduction (SCR) using hydrocarbons or ammonia is a promising technology for post-combustion treatment of NO_x [4]. Transition metal-containing ZSM-5 zeolites have been extensively investigated as possible candidates for SCR catalysts [5,6]. However, studies on transition metal ZSM-5 have shown that there are limitations of these transition metal zeolite catalysts for deNO_x such that deactivation occurs under typical conditions of humid, oxygen rich exhaust streams [7].

Despite its sensitivity to even trace amounts of water, zeolite Y has attracted a great deal of attention as a NO_x storage-reduction (NSR) catalyst [8–12]. Several recent studies used alkali and/or alkaline earth substituted Y zeolites as SCR catalysts for NO_x reduction [10,13,14]. In the absence of transition metals, zeolite Y could offer novel SCR pathways different from those that occur in transition metal ZSM-5 catalysts. Yeom and co-workers have investigated the reactions between hydrocarbons and NO_2 in BaNaY with FT-IR spectroscopy [13]. Their results show that the formation of ammonium nitrite (NH_4NO_2) is a crucial step for SCR reactions in zeolite Y. A parallel pathway involving free radicals was also mentioned as potentially being important. Previously, we investigated the selective catalytic reduction of NO_2 with propylene in nanocrystalline NaY zeolite with a crystal size around 80 nm [15]. In the absence of oxygen, complete reduction of NO_2 to N_2 and O_2 occurred at relatively low temperatures ($T \leq 473$ K) according to reaction **1**.

$$3NO_2 + C_3H_6 = 3CO + (3/2)N_2 + 3H_2O \qquad (1)$$

As we have recently discussed, nanocrystalline Y zeolites may be particularly useful in environmental applications due to the small crystal size and large internal *and* external surface areas [16]. Since NO_x is mainly stored as adsorbed nitrate and nitrite in zeolite Y, the high total surface area of nanocrystalline zeolites could offer additional advantages for NO_x storage. Furthermore, the small crystal size of nanocrystalline zeolites can dramatically alter the diffusional properties of these materials. The dependence of the SCR reaction rate, NO_x conversion and catalyst durability on zeolite crystal size has been previously reported by others [17–21]. Ogura and co-workers reported the dependence of catalytic activity on H-ZSM-5 crystal size in deNO_x reactions [17]. Tabata and co-workers studied the intra crystalline diffusion of NO in ZSM-5 zeolites with different crystal sizes [20]. Higher conversion of NO_x and propane in SCR reactions was obtained over zeolites with a smaller crystal size. Shichi and co-workers discovered that the reaction rate and conversion of NO_x in SCR reaction over MFI-type zeolite were influenced by intracrystalline diffusion of hydrocarbons [18,19]. In addition, it has been reported that the durability of Co/HZSM-5 increased with decreasing crystal size [21]. With small crystal size and large external surface area, nanocrystalline zeolites can provide additional adsorption/reaction sites with diverse functionality and diffusional advantages.

In the work described here, *in situ* transmission FT-IR spectroscopy is used to investigate propylene-SCR of NO_2 over nanocrystalline NaY zeolite at low

* To whom correspondence should be addressed.
E-mail: sarah-larsen@wiowa.edu; vicki-grassian@uiowa.edu

temperature ($T = 473$ K). The zeolite crystal size used in this study is 23 nm. This represents the smallest nanocrystalline NaY zeolite material reported in the literatures or used in any SCR reaction. The performance of nanocrystalline NaY zeolite in SCR reactions is compared to commercial NaY zeolite with a larger particle size in order to explore the potential advantage of the small crystal size of nanocrystalline NaY zeolite and to determine if differences in the chemical as well as physical properties of nano-sized zeolite are important in SCR reactions.

2. Experimental section

2.1. Zeolite sample preparation and materials

Nanocrystalline NaY zeolite was synthesized using clear solutions according to the method reported by Creaser and coworkers [22]. Sodium hydroxide, aluminum isopropyloxide, tetramethylammonium hydroxide (TMAOH) and distilled water were mixed and stirred until the resulting mixture became a clear solution. Then tetraethyl orthosilicate (TEOS) was added to the clear solution. The clear solution mixture was stirred overnight to ensure complete hydrolysis of the aluminum and silicon sources. The final clear synthesis gel had the following composition: 0.07Na : 2.4TMAOH : 1.0Al : 2.0Si : 132H_2O : 3.0i-PrOH : 8.0EtOH, the latter two alcohols came about from the hydrolysis of the aluminum isopropyloxide and TEOS, respectively. In order to optimize the formation of small NaY crystals, the sodium content was intentionally set too low relative to aluminum content in the synthesis gel. Previous results have shown that a low Na/Al ratio (less than approximately 0.1) favors the formation of small NaY crystals and limits the formation of NaA [22]. The clear solution was transferred into a 500 mL flask equipped with an air cooled condenser and was heated to $T = 368$ K in an oil bath for 84 h with stirring. Nanocrystalline Y powders were recovered from the milky, colloidal suspension of NaY after two cycles of centrifugation, washed with deionized water and dried at $T = 393$ K in air. The nanocrystalline NaY sample was calcined at $T = 773$ K under oxygen flow for 16 h to remove organic templates.

The synthesized nanocrystalline NaY zeolite and the commercial NaY zeolite purchased form Aldrich were characterized by several different techniques including scanning electron microscopy (SEM), X-ray diffraction (XRD), nitrogen adsorption isotherms and solid state NMR [16]. Representative SEM images of nanocrystalline and commercial NaY zeolite are shown in figure 1. The average crystal size of nanocrystalline NaY zeolite was determined to be 23 nm [16]. The commercial NaY zeolite is composed of large intergrown NaY crystals with diameters of ~ 1 μm. The external, internal and total surface areas of nanocrystalline NaY zeolite were determined to be 178, 406 and 584 m^2/g, respectively. The total surface area of commercial NaY zeolite was 477 m^2/g and as discussed in previous work [16], the external surface area of commercial NaY zeolite is estimated from the crystal size to be ~ 4 m^2/g. The Si/Al ratios of nanocrysatlline NaY and commercial NaY zeolite were determined to be 1.8 and 2.0, respectively [16].

Aluminum isopropyloxide, tetraethyl oxyorthosilane (TEOS) and sodium hydroxide were purchased from Alfa Aesar. Commercial NaY zeolite and tetramethylammonium hydroxide (TMAOH) solution (20 wt%) were purchased from Aldrich. Research-grade purity oxygen and carbon dioxide were purchased from Air Products. Research-grade purity nitrogen dioxide, propylene, nitric oxide, nitrous oxide and carbon monoxide were purchased from Matheson. All gases were used without further purification. 2,6-Di-tert-butylpyridine (DTBPy, 97%) purchased from Aldrich and pyridine (99.9%) purchased from Fisher Scientific were further dehydrated over molecular sieves and subjected to several freeze-pump-thaw cycles.

2.2. Fourier transform infrared spectroscopy

The infrared sample cell used in this study has been described previously [23]. Seven milligram of NaY zeolite was mixed with water and the resulting hydrosol was coated onto a 3×2 cm^2 photoetched tungsten grid held

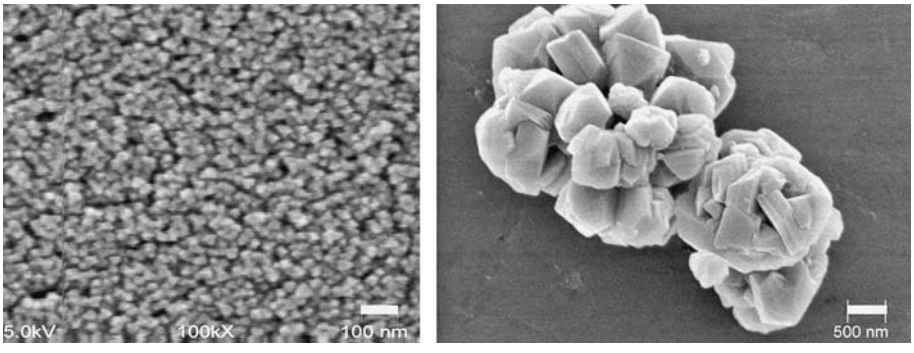

Figure 1. SEM images of nanocrystalline NaY zeolite (scale bar = 100 nm) and commercial sample of NaY zeolite (scale bar = 500 nm).

in place by nickel jaws. The nickel jaws are attached to copper leads so that the sample can be resistively heated. A thermocouple wire attached to the tungsten grid is used to measure the temperature of the sample. The tungsten grid with zeolite sample is placed inside of a stainless steel cube. The cube has two BaF_2 windows for infrared measurements and is connected to a vacuum/gas handling system.

The stainless steel IR cell is held in place by a linear translator inside the sample compartment of a Mattson Galaxy 6000 infrared spectrometer equipped with a narrowband MCT detector. The linear translator allows each half of the sample grid to be moved into the infrared beam path. This allows the detection of gas phase and adsorbed species in zeolites to be obtained under identical reaction conditions. Each absorbance spectrum shown is obtained from referencing 64 scans at an instrument resolution of 4 cm^{-1} to the appropriate background of the clean zeolites or the blank grid, unless otherwise noted.

The NaY sample was gradually heated under vacuum at $T=623$ K or higher temperature overnight to remove adsorbed water. Reactant gases were loaded into the zeolite through the gas handling system. Two absolute pressure transducers were used to monitor the pressure. The extinction coefficient of individual gases was calibrated using the characteristic IR absorption band and measuring the pressure using an absolute pressure transducer in the pressure range from 30 mTorr to 3 Torr. Typically, the zeolite was equilibrated with gases prior to a spectrum being recorded. In pyridine (or DTBPy) adsorption experiments, adsorption was carried out by equilibrating the zeolite powder with 1 Torr pressure of pyridine (or DTBPy) vapor at $T=473$ K. The sample was then evacuated for 30 min at $T=473$ K and cooled back to room temperature prior to recording a spectrum.

In SCR reactions, NO_2 and propylene (1:1 mole ratio) were first mixed in a chamber before being introduced into the IR cell at room temperature. Thirty minutes were allowed for adsorption equilibrium before an excess amount of oxygen was added into the IR cell. Time course experiments were conducted by automatically recording infrared spectra of the NaY zeolite or gas phase every 5 s. In experiments designed to determine the effect of adsorbed water on the SCR reaction, NaY zeolite was exposed to 0.2 Torr of water vapor before loading reactant gases.

3. Results and discussion

3.1. Propylene-SCR of NO_2 in NaY zeolite at $T=473$ K: gas phase product distribution

The gas-phase product distributions were measured by IR before and after propylene-SCR of NO_2 in NaY (nanocrystalline and commercial) at $T=473$ K and the results are summarized in table 1. Gas-phase NO_2 was not observed after adsorbing the reactant gases for 30 min at room temperature in nanocrystalline NaY or in commercial NaY zeolite. However, NO, N_2O, and C_3H_6 were evident in the gas phase. More nitrogen products (NO and N_2O) and more propylene were observed in the gas phase on commercial NaY compared to nanocrystalline NaY zeolite suggesting that more NO_2 and propylene were adsorbed or reacted in the nanocrystalline NaY zeolite. It can be seen from the data in table 1 that water markedly decreased the adsorption capacity of propylene in nanocrystalline NaY zeolite. The surface sites in nanocrystalline NaY zeolite may be poisoned by water due to hydrogen bonding with silanol groups on the external surface, which are important adsorption sites for NO_x and propylene [15]. The effect of adsorbed water on the adsorption capacity of NO_2 and propylene in the commercial sample is much smaller compared to the nanocrystalline NaY zeolite.

Next, propylene-SCR of NO_2 in nanocrystalline and commercial NaY zeolite was carried out at $T=473$ K in the presence of an excess amount of oxygen. After 6 h of SCR, no gas-phase NO_2 or NO was observed indicating that conversion of gas-phase NO_x (combined gas-phase NO_2 and NO concentrations) was 100% in nanocrystalline NaY zeolite in the absence of adsorbed water. N_2O was the major N-containing gas-phase product detected with FT-IR spectroscopy. In SCR reactions over the commercial NaY zeolite, 44% of total loaded NO_2 was converted into NO and the selectivity toward N_2O formation was 14% compared to 52% for nanocrystalline NaY zeolite. The relatively high concentration of propylene and low concentration of CO_2 in the gas phase after SCR reactions also indicate that propylene-SCR of NO_2 using commercial sample did not occur to the same extent as in nanocrystalline NaY zeolite. Based on the nitrogen mass balance, the selectivity toward N_2 formation was estimated to be approximately 20% in SCR reactions using nanocrystalline and commercial NaY zeolite as the catalyst. CO_2 was the major carbon-containing gas-phase product, while CO was detected as the other gas-phase carbon-containing product with a concentration lower than 15 μmol L^{-1}.

Table 1
Concentration (μmol L^{-1}) of gas-phase components before and after propylene-SCR of NO_2 in 7 mg NaY zeolite at $T=473$ K for 6 h

Catalyst	Before SCR			After SCR			
	NO	N_2O	C_3H_6	NO	N_2O	C_3H_6	CO_2
Nanocrystalline NaY	6	1	11	0	18	4	174
Nanocrystalline NaY with H_2O	18	2	37	11	13	33	48
Commercial NaY	16	1	31	31	5	22	52
Commercial NaY with H_2O	13	1	37	28	7	21	60

The loadings of both NO_2 and C_3H_6 are 70 ± 5 μmol L^{-1}; the concentration of oxygen in the IR cell is 550 ± 20 μmol L^{-1}.

Adsorbed water markedly decreased the activity and selectivity of the nanocrystallline NaY zeolite catalyst. In SCR reaction over nanocrystalline NaY zeolite with adsorbed water, the selectivity toward NO and N_2O formation was ~14% and ~36%, respectively, compared to 0% and ~52% in the absence of adsorbed water. Complete oxidation of propylene into CO_2 was severely inhibited by adsorbed water in nanocrystalline NaY zeolite. This is indicated by the relatively high concentration of propylene and low concentration of CO_2 in the gas phase after SCR reaction in nanocrystalline NaY zeolite in the presence of adsorbed water. Adsorbed water did not appear to influence the reactivity of the commercial NaY sample to any great extent.

In order to understand these differences between the propylene-SCR of NO_2 in nanocrystalline NaY zeolite and the commercial NaY zeolite, FT-IR spectroscopy was further used to probe the nature of adsorbed surface species. Specifically, FT-IR spectroscopy was used to: (i) probe the nature of external surface sites for the nanocrystalline NaY zeolite; (ii) identify differences in NO_2 adsorption in nanocrystalline NaY zeolite and commercial NaY at $T=298$ K; (iii) identify differences in NO_2 and C_3H_6 co-adsorption in nanocrystalline NaY zeolite and commercial NaY at $T=298$ K.

3.2. *Nature of external surface sites on nanocrystalline NaY zeolite*

As recently discussed, FT-IR analysis revealed several differences between nanocrystalline NaY zeolite and commercial NaY zeolite [16]. Figure 2 shows the FT-IR spectra of nanocrystalline NaY zeolite and commercial sample after being heated overnight under vacuum at $T=623$ K. In the spectrum of nanocrystalline NaY zeolite, three absorptions are observed in the spectral region between 3765 and 3630 cm^{-1}. The most intense and highest frequency band at 3744 cm^{-1} is assigned to terminal silanol groups that are on the external surface of the zeolite crystals [16]. This feature is of much weaker intensity in the commercial NaY sample as expected since the external surface area is ~40 times smaller than the nanocrystalline NaY sample. Previously it was shown that silanol groups on the external surface of nanocrystalline NaY zeolite are important adsorption sites for NO_x and propylene in SCR reactions [15]. The absorption band at 3695 cm^{-1} is assigned to hydroxyl groups attached to Na^+ [24].

In the FT-IR spectrum of nanocrystalline NaY zeolite (figure 2), the band at 3656 cm^{-1} is associated with hydroxyl groups attached to extra framework alumina (EFAL) species [25]. Pyridine adsorption experiments coupled with FT-IR analysis have revealed the existence of Bronsted acid sites as well as Lewis acid sites associated with EFAL species only present in nanocrystalline NaY zeolite [16]. In order to determine the location of the EFAL species, adsorption of pyridine and 2,6-Di-tert-butylpyridine (DTBPy) in nanocrystalline NaY zeolite was conducted. It has been suggested that most EFAL species are located on the external surface of zeolite Y [26,27]. While pyridine can adsorb into the

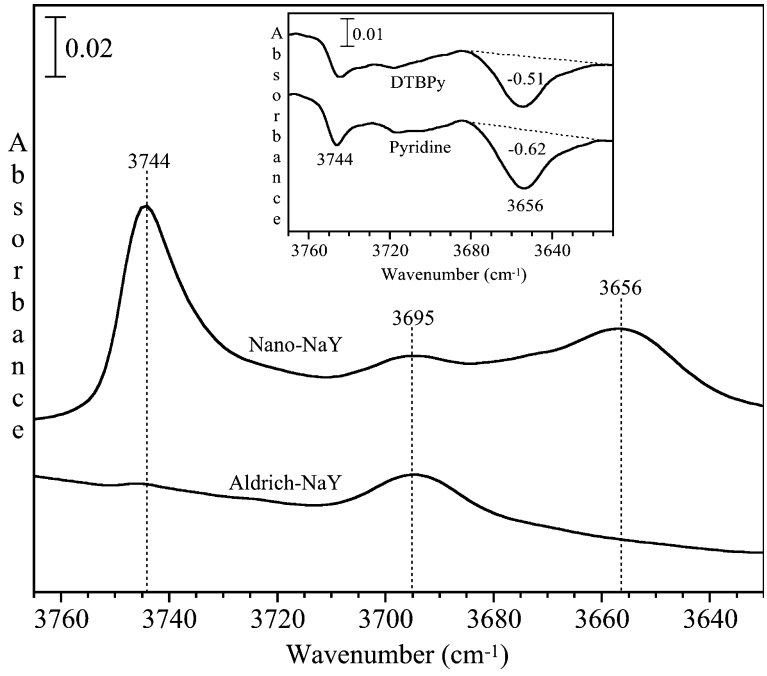

Figure 2. FT-IR spectra of surface hydroxyl groups in nanocrystalline NaY and commercial NaY zeolite after heating to $T=623$ K overnight under vacuum. The blank grid is used as a reference. The inset shows the difference spectra following DTBPy and pyridine adsorption in nanocrystalline NaY zeolite. The absorbance spectra prior to DTBPy or pyridine adsorption are subtracted from the spectra after the adsorption. The negative peaks show the loss of hydroxyl groups due to adsorption or reaction with these probe molecules. All spectra were recorded at $T=298$ K.

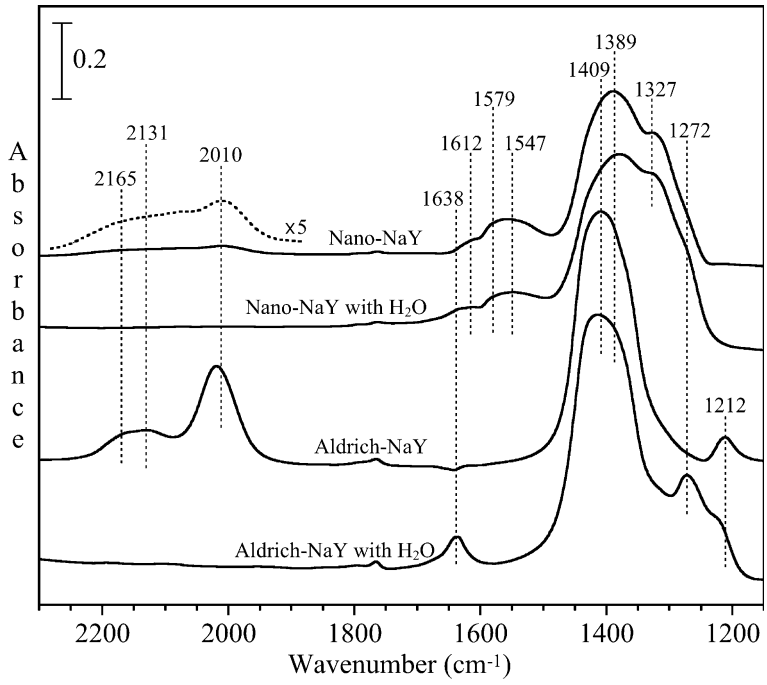

Figure 3. FT-IR spectra of 0.5 Torr NO_2 adsorbed in nanocrystalline NaY and commercial NaY zeolite in the presence and absence of 10 μmol adsorbed water at $T = 298$ K. All spectra shown in figure 3 use the corresponding clean NaY zeolite prior to adsorption as a background. In addition, gas-phase absorptions have been subtracted from each of the FT-IR spectra.

zeolite pores, DTBPy can only interact with the hydroxyl groups on the external surface (and in the pore mouth region) of the zeolites since its kinetic diameter is larger than the pore opening of Y zeolites [28]. Thus DTBPy was used as a probe molecule to characterize acid sites located on the external surface of the zeolites [28]. The difference FT-IR spectra after pyridine and DTBPy adsorption on nanocrystalline NaY zeolite are shown in figure 2 (inset). The integrated absorbance of the negative peak at 3656 cm^{-1} is approximately proportional to the amount of EFAL species with Bronsted acidity in nanocrystalline NaY zeolite. After DTBPy and pyridine adsorption on nanocrystalline NaY zeolite, the integrated absorbance of the negative peak at 3656 cm^{-1} are −0.51 and −0.62, respectively. Therefore, it can be concluded that more than 80% of the EFAL species with Bronsted acidity are located on the external surface of nanocrystalline NaY zeolite.

3.3. Adsorption of NO_2 in NaY zeolite at $T = 298$ K

FT-IR analysis of NO_2 adsorption was conducted in the absence and presence of adsorbed water. Figure 3 shows the difference FT-IR spectra of nanocrystalline and commercial NaY zeolite in the presence of 0.5 Torr NO_2 at $T = 298$ K. Gas-phase absorptions have been subtracted from the spectra shown in figure 3 to highlight the spectra of the adsorbed species. The assignment of the adsorbed species in the zeolite can be based on several earlier studies [8,10,11,15,29]. It is well known that nitrate (NO_3^-) and nitrosonium ion (NO^+) were produced *via* the NO_2 disproportionation (reaction **2**) in zeolite Y in the absence of adsorbed water.

$$2NO_2 \rightarrow NO_3^- + NO^+ \qquad (2)$$

In the spectra shown in figure 3, the broad absorption bands near 1409 and 1389 cm^{-1} can be assigned to the v_3 mode of nitrate ions attached to Na^+ sites [10,11]. The absorption bands at 1612, 1579 and 1547 cm^{-1} are associated with the v_3 mode of adsorbed nitrate bonded in different coordinations (bridging, bidendate and monodentate, respectively) on the EFAL sties in nanocrystalline NaY zeolite [15,30]. The absorption at 1327 cm^{-1} is also associated with nitrate adsorption on EFAL sites [15]. The absorption bands at 2131 and 2010 cm^{-1} are assigned to nitrosonium ions adsorbed onto different cationic positions in the zeolite framework [10,11]. Another absorption feature at 2165 cm^{-1} can be attributed to the N–O stretching mode from $[NO^+][NO_2]$ or $[NO^+][N_2O_4]$ adducts adsorbed on Lewis base sites [10,11]. An absorption feature at 1212 cm^{-1} readily observed only in the FT-IR spectra of NO_2 adsorbed in commercial NaY sample indicates the formation of nitrosyl ion (NO^-) [29], which adsorbs on surface cationic sites.

A comparison of the spectrum of NO_2 adsorbed in nanocrystalline and commercial NaY zeolite shows several differences. These include: (1) nitrate absorptions due to nitrate adsorbed on EFAL sites for nanocrystalline NaY zeolite but not for the commercial NaY sample; (2) the NO^+ absorption bands between 1900

and 2300 cm^{-1} in the spectrum of NO_2 adsorbed in commercial NaY zeolite are 5 times more intense compared to those in nanocrystalline NaY zeolite (see figure 3); (3) broader absorption bands in spectrum of the nanocrystalline NaY relative to the commercial NaY sample.

Nitrate adsorbed on EFAL sites is only observed in nanocrystalline NaY zeolite. This can be understood from the characterization studies discussed above and that the nanocrsytalline NaY zeolite has a much greater external surface area compared to commercial NaY zeolite. Since EFAL are associated with external surface, there is a much greater number of these sites per unit weight for nanocrystalline NaY zeolite compared to commercial NaY zeolite. The FT-IR spectra shown in figure 2 also confirm the presence of EFAL sites for nanocrystalline NaY zeolite. The difference in the intensity of NO^+ bands between nanocrystalline and commercial NaY zeolite may also be understood in terms of EFAL sites. In nanocrystalline NaY zeolite, NO_2 adsorption in part occurs on cationic sites of EFAL species (M^{n+}–O^{2-}) without the production of NO^+, according to reaction **3** [10].

$$M^{n+} - O^{2-} + NO_2 \rightarrow M^{n+} - NO_3^- \qquad (3)$$

Furthermore, the FT-IR spectra of SCR surface species in nanocrystalline NaY show additional broadening of the absorption bands and a greater degree of spectral overlap and interference relative to those in the commercial NaY sample. This suggests that the surface adsorption sites in nanocrystalline NaY zeolite are more heterogeneous than in commercial NaY zeolite. In commercial NaY zeolite, the internal surface provides most of the adsorption sites and Na^+ is the only cationic site. In nanocrystalline NaY zeolite, this is not the case as the external surface accounts for ~30% of the total surface. The silanol groups and EFAL species on the external surface of nanocrystalline NaY zeolite provide further surface sites [16].

FT-IR spectra of NO_2 adsorption in the presence of adsorbed water were recorded and several differences were noted. Nitrosonium ion did not form in NaY zeolites which contained adsorbed water. Instead, an absorption peak at 1272 cm^{-1} associated with adsorbed nitrite (NO_2^-) was identified in the FT-IR spectra of surface NO_x species formed upon exposing of 0.5 Torr pressure of NO_2 to NaY zeolites (figure 3). In the presence of surface adsorbed water (as indicated by the H_2O bending mode absorption at 1638 cm^{-1}), NO_2 reacts preferentially according to reaction **4** [12,15].

$$2NO_2 + H_2O \rightarrow HNO_3 + HONO \qquad (4)$$

The nitric and nitrous acids deprotonate and adsorb on surface cationic sites to form surface nitrate and nitrite.

In summary, nanocrystalline NaY zeolite with a much smaller crystal size and a larger external surface area compared to commercial zeolite sample results in more silanol groups and more EFAL species located on external surface of nanocrystalline NaY zeolite. These external surface sites play an important role in the adsorption of NO_2 in the nanocrystalline zeolite mate-

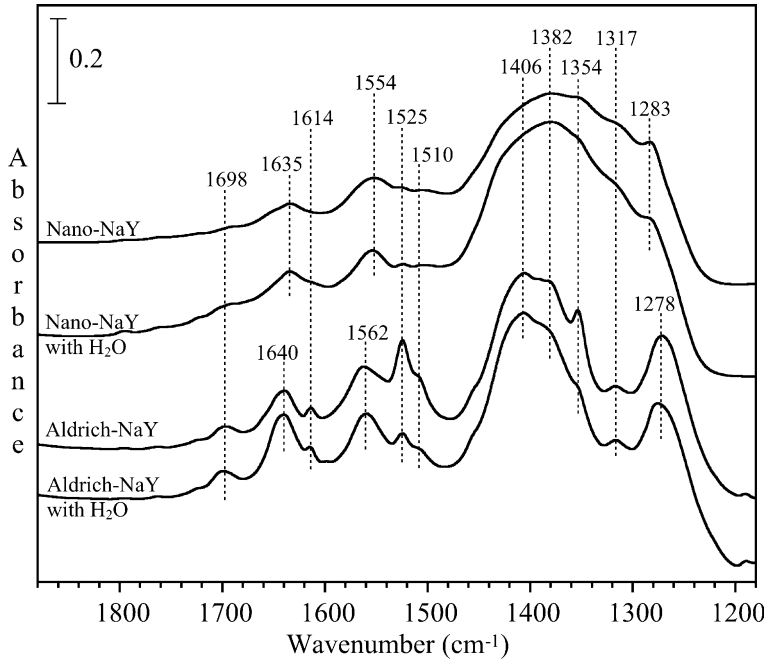

Figure 4. FT-IR spectra of nanocrystalline NaY and commercial NaY zeolite in the presence and absence of adsorbed water at $T = 298$ K following the co-adsorption of NO_2 and C_3H_6 (1:1) mixture. All spectra shown in figure 4 use the corresponding clean NaY zeolite prior to adsorption as a background. In addition, gas-phase absorptions have been subtracted from each of the FT-IR spectra.

rials and are easily poisoned by water as will be discussed in the next sections [15,16].

3.4. Co-adsorption of NO_2 and C_3H_6 in NaY zeolite at $T = 298$ K

To further understand the differences in the potential of nanocrystalline NaY zeolite in deNO_x catalysis compared to the commercial NaY sample, the co-adsorption of NO_2 and C_3H_6 was investigated. NO_2 and C_3H_6 were first mixed (1:1 mole ratio) in a chamber prior to being introduced into the IR cell at $T = 298$ K. Thirty minutes was allowed for adsorption equilibrium. The FT-IR spectra of resulting surface species in nanocrystalline NaY zeolite and commercial zeolite sample are shown in figure 4.

Although there are considerable spectral overlap and interference, several surface species can be identified based on previous reports in the literature. In the spectra shown in figure 4, adsorbed oxygenated hydrocarbons ($C_xH_yO_z$) can be identified by several absorptions near 1698, 1614, 1525, 1510, 1354, and 1317 cm^{-1}. For example, carbonyl containing compounds (ν(C=O) at 1698 cm^{-1}) may come about from the direct oxidation of adsorbed propylene by NO_3^- [31–33]. Two bands at 1525 and 1510 cm^{-1} are most likely due to the formation of monodentate carbonate ions and formate ions, respectively [34]. The absorption at 1614 cm^{-1} can be assigned to carboxylic acids. The absorption peaks at 1354 and 1317 cm^{-1} can be assigned to surface CH_x species [13]. A number of nitrogen containing surface species can also be identified in the spectra shown in figure 4. The broad band with a maximum at 1406 cm^{-1} characterizes nitrate species adsorbed on Na^+ sites as discussed in the previous section. An absorption feature near 1382 cm^{-1} most likely is due to the formation of Na^+-nitrate, organic nitro compound and/or surface CH_x species [15].

In the spectrum of nanocrystalline NaY zeolite after NO_2 and C_3H_6 adsorption (figure 4), two relatively intense absorption bands at 1554 and 1635 cm^{-1} are also apparent. Yeom and co-workers investigated the adsorption and reactions of nitromethane in zeolite Y [13]. With the aid of isotopic labeling, nitromethane and methyl nitrite were identified with absorption peaks at 1556 and 1653 cm^{-1}, respectively. Therefore, the absorption at 1554 cm^{-1} can be assigned to organic nitro species [15]. The broad peak at 1635 cm^{-1}, however, cannot be definitely assigned to a single compound based on the infrared data presented here. It may include the contribution from ν(ONO) mode of organic nitrito compounds, ν(C=C) mode of adsorbed propylene and/or bending mode of adsorbed water. The relatively intense band at 1283 cm^{-1} should be associated with ν(C-O) mode of organic nitrito compounds [15,35].

In the spectra of surface species adsorbed in commercial NaY zeolite, organic nitro compounds can be identified by the absorption band at 1562 cm^{-1}. Similarly, the broad band at 1640 cm^{-1} may include the contribution from ν(ONO) mode of organic nitrito compounds, ν(C=C) mode of adsorbed propylene and/or bending mode of adsorbed water. The absorption band at 1278 cm^{-1} should also be associated with organic nitrito compounds. A difference of 5–8 cm^{-1} is observed between the absorption bands of the nitro/nitrito compounds adsorbed in nanocrystalline NaY zeolite and the commercial NaY sample. In nanocrys-

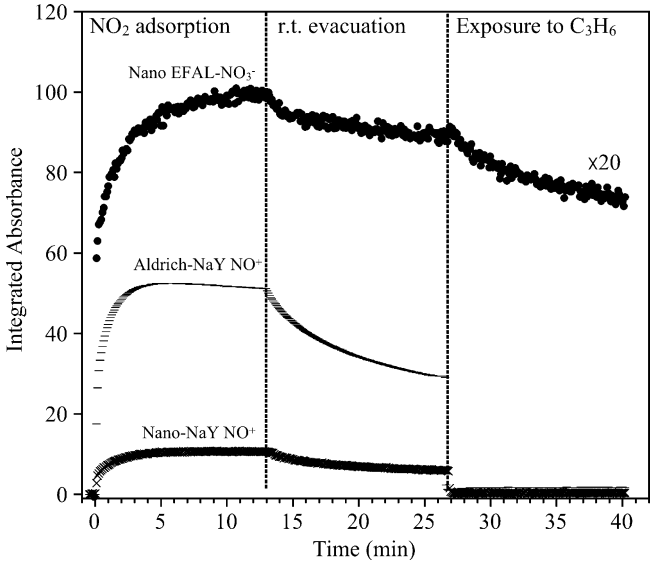

Figure 5. The integrated absorbance of surface NO_3^- on EFAL sites (●), NO^+ (×) in nanocrystalline NaY zeolite and NO^+ (–) in commercial NaY zeolite as a function of time. The changes of the integrated absorbance are shown in the process of NO_2 adsorption, evacuation of the IR cell and exposure of propylene to the surface species in the zeolites. Spectra used for band integration were recorded every 5 s. The integrated absorbance of surface NO_3^- on EFAL sites in nanocrystalline NaY zeolite is 20 times larger than the original absorbance.

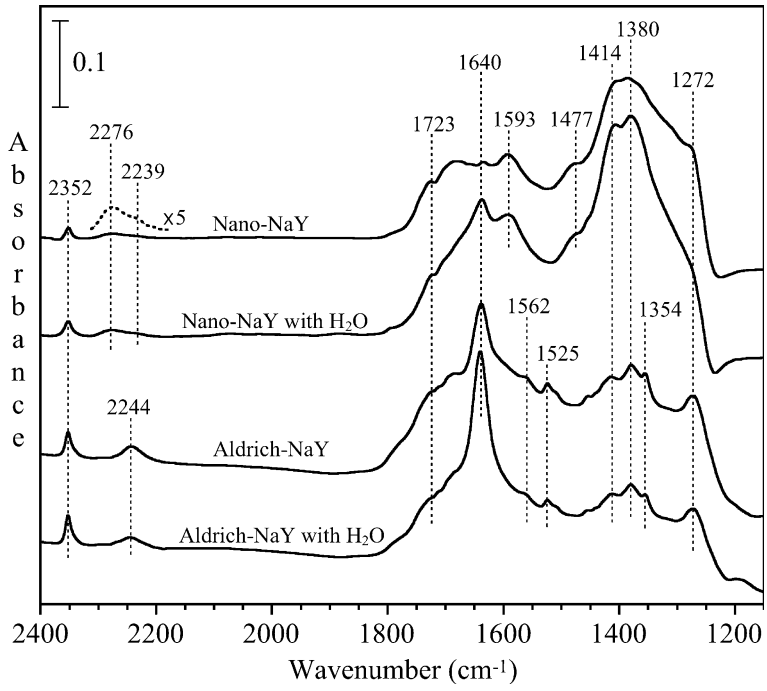

Figure 6. FT-IR spectra of adsorbed species following propylene-SCR of NO_2 at $T=473$ K for 6 h in nanocrystalline NaY and commercial NaY zeolite in the presence and absence of adsorbed water. The spectra were recorded at $T=298$ K. All spectra shown in figure 6 use the corresponding clean NaY zeolite prior to adsorption as a background. In addition, gas-phase absorptions have been subtracted from each of the FT-IR spectra.

talline NaY zeolite, organic nitro/nitrito compounds most likely formed over EFAL species on the external surface [15].

Slight differences are observed between the FT-IR spectra of SCR surface species in NaY zeolites in the absence and presence of adsorbed water (figure 4). For example, it is known that water suppresses the formation and/or promoted the desorption of carbonate ion (1525 cm^{-1}) and formate ions (1510 cm^{-1}) [36]. This can be seen in the spectra shown in figure 4 for commercial NaY zeolite.

The reactivity of surface NO_x species towards propylene at room temperature was also investigated with FT-IR spectroscopy. First, the NaY zeolite sample was equilibrated with 0.5 Torr NO_2, followed by evacuating the IR cell under 10^{-3} Torr vacuum at room temperature. Then the surface NO_x species remaining in the zeolite sample were exposed to 0.5 Torr C_3H_6 at room temperature. The reactivity of surface NO_x species towards propylene was quantitatively characterized by integrating the individual absorption band in the FT-IR spectra recorded in the NO_2 adsorption-evacuation-C_3H_6 exposure process, as shown in figure 5.

Figure 5 indicates that NO^+ in both nanocrystalline and commercial NaY zeolite is very reactive toward C_3H_6 at room temperature. 44% of NO^+ in nanocrystalline NaY zeolite and 42% of NO^+ in the commercial NaY sample were gone after being evacuated at room temperature for 13 min. All of the nitrosonium ions disappeared immediately in contact with C_3H_6 at room temperature. The high reactivity of NO^+ in NaY zeolite toward molecules such as H_2O and C_3H_6 has been reported previously [12,15]. NO_3^- adsorbed on EFAL sites in nanocrystalline NaY zeolite also displays high reactivity toward propylene at room temperature. As shown in figure 5, 10% of the NO_3^- on EFAL sites in nanocrystalline NaY zeolite was pumped away from the zeolite during the evacuation process. Another 16% loss of the NO_3^- on EFAL sites was observed upon exposure of propylene to nanocrystalline NaY zeolite at room temperature. Considering the fact that the formation of several SCR surface species (such as organic nitro and nitrito compounds) in this process can contribute to the absorption bands in the same spectral region as NO_3^- on EFAL sites in the FT-IR spectra, the actual loss of NO_3^- on EFAL sites upon exposure of C_3H_6 is most likely more than 16%. In both nanocrystalline and commercial NaY zeolite samples, the intensity of NO_3^- on Na^+ sites barely changed in contact with C_3H_6, indicating the low activity of NO_3^- on Na^+ sites toward C_3H_6 at room temperature. The reactivity of NO_3^- on EFAL sites toward C_3H_6 is consistent with the fact that organic nitro and nitrito compounds formed preferentially on EFAL sites in nanocrystalline NaY zeolite in the co-adsorption of NO_2 and C_3H_6, as discussed previously (figure 4).

3.5. Adsorbed products following propylene-SCR of NO_2 in NaY zeolite at $T = 473$ K

At elevated temperature, organic nitro and nitrito compounds can be converted into organic isocyanate [15]. In this study, the formation of isocyanic acid and organic isocyanate on EFAL sites is observed when nanocrystalline NaY zeolite was used as the SCR catalyst. The FT-IR spectra of surface species after SCR reactions in both nanocrystalline and commercial NaY zeolite are shown in figure 6. After propylene-SCR of NO_2 at $T = 473$ K for 6 h in nanocrystalline NaY zeolite, two surface species can be identified as characterized by the absorption bands at 2276 and 2239 cm^{-1}, respectively. The absorption band at 2276 cm^{-1} has been assigned to isocyanic acid [13,15]. The other band at 2239 cm^{-1} has been assigned to organic isocyanate in several previous studies using alumina-supported materials as SCR catalysts [37–42]. Since a substantial amount of EFAL species is detected in nanocrystalline NaY zeolite used in this study, the band at 2239 cm^{-1} should be associated with organic isocyanate on EFAL sites. Isocyanic acid and organic isocyante most likely came from the thermal reactions of organic nitro/nitrito compounds. When commercial NaY zeolite was used as the SCR catalyst, organic isocyante was produced as characterized by an absorption band at 2244 cm^{-1} in the spectra shown in figure 6.

Other absorption features shown in figure 6 can be assigned based on the discussion in the previous section and relevant reports in the literature. Nitrate remained in NaY zeolite after SCR reactions can be identified by two absorption bands at 1414 and 1380 cm^{-1} [10,11,15]. Carbon atom-containing surface species can be identified by the absorption bands at 1723, 1593 and 1477 cm^{-1} in nanocrystalline NaY zeolite and 1723, 1525 and 1354 cm^{-1} in commercial sample [15,43]. Since acetic acid adsorbed in NaY zeolite gave rise to absorption bands at 1722 and 1271 cm^{-1}, the absorption features at 1723 and 1272 cm^{-1} should be assigned to carboxylic acid. However, the absorption band at 1272 cm^{-1} may partly attribute to the formation of nitrite, considering the fact that adsorbed water (bending mode at 1640 cm^{-1}) was observed in both nanocrystalline and commercial NaY samples. As mentioned previously, nitrite formed upon adsorption of NO_2 in NaY zeolites in the presence of adsorbed water (figure 3). An absorption band at 1562 cm^{-1} characterizing organic nitrito compounds, which is considered as one of the important SCR intermediates, is evident in the spectra of commercial NaY zeolite after SCR reactions at $T = 473$ K for 6 h. Surface adsorbed CO_2 can be identified by the absorption band at 2352 cm^{-1} in the spectra shown in figure 6 [44].

It has been reported isocyanic acid can be generated in the reactions between organic nitro compound and gas-phase NO_x [13]. Isotopic labeling studies have shown that one nitrogen atom in N_2 originates from the gas-phase NO_x and the other nitrogen atom originates from a surface nitrogen-containing species in SCR reactions [45]. In nanocrystalline NaY zeolite, the reactions between gas-phase NO_x and surface NCO compounds or their hydrolysis products (such as ammonium ions) on EFAL sites are important for the N–N bond formation to produce N_2 and N_2O. Compared to surface sites in commercial NaY zeolite, EFAL species on the external surface of nanocrystalline NaY zeolite yield chemically distinct adsorption and reaction sites in SCR reactions.

It should be noticed that a greater amount of adsorbed water is observed in the FT-IR spectra of commercial NaY zeolite after SCR reactions relative to those of nanocrystalline NaY zeolite (figure 6). The accumulation of surface adsorbed water in commercial NaY zeolite during the SCR reactions (figure 6) might indicate that hydrolysis of isocyanate did not occur in the commercial NaY sample to the same extent as it does in nanocrystalline NaY zeolite. Supporting this is the fact that more NO but less N_2O formation was observed after propylene-SCR of NO_2 in commercial NaY zeolite compared to that happened in nanocrystalline NaY zeolite (table 1). In addition, SCR reactions in nanocrystalline NaY zeolite are more sensitive to adsorbed water than in commercial sample, as shown by the comparison in table 1. Most likely, water generated in SCR reactions over nanocrystalline NaY zeolite reacted with surface SCR intermediates (such as organic isocyanate), and did not inhibit the further adsorption of gas-phase NO_x and C_3H_6. Pre-adsorbed water in nanocrystalline NaY zeolite before starting SCR reactions, however, strongly inhibited the adsorption of NO_2 and C_3H_6 *via* poisoning adsorption sites on external surface and further SCR reactions. In commercial NaY zeolite, external surface did not play an important role in SCR reactions at $T = 473$ K. Consequently, pre-adsorbed water did not have a significant effect on propylene-SCR of NO_2.

4. Conclusions

Compared to commercial NaY zeolite with a larger particle size, nanocrystalline NaY zeolite demonstrated markedly higher adsorption capacity and activity toward N–N bond formation in propylene-SCR of NO_2 at low temperature ($T = 473$ K). FT-IR analysis suggests that a significant amount of SCR reactions in nanocrystalline NaY zeolite occurred on the external surface. The study on the reactivity of surface NO_x species in nanocrystalline NaY zeolite indicated that EFAL sites in nanocrystalline NaY zeolite were responsible for the higher NO_x ($NO_2 + NO$) conversion and higher selectivity toward N_2O formation in SCR reactions. However, nanocrystalline NaY zeolite is more sensitive to adsorbed water in propylene-SCR of NO_2 at $T = 473$ K

relative to commercial NaY zeolite. Most likely, adsorbed water poisons important surface adsorption sites by hydrogen bonding to silanol groups on the external surface of nanocrystalline NaY zeolite.

Acknowledgments

The authors thank Dr. Weiguo Song for providing the nanocrystalline NaY zeolite sample and the SEM images. Although the research described in this article has been funded wholly or in part by the Environmental Protection Agency through grant number EPA R829600 to SCL and VHG, it has not been subjected to the Agency's required peer and policy review and therefore does not necessarily reflect the views of the Agency and no official endorsement should be inferred.

References

[1] C.S. Cundy and P.A. Cox, Chem. Rev. 103 (2003) 663.
[2] T.F. Degnan Jr., Top. Catal. 13 (2000) 349.
[3] G. Delahay and B. Coq, Catal. Sci. Ser. 3 (2002) 345.
[4] S. Bhattacharyya and R.K. Das, Int. J. Energy Res. 23 (1999) 351.
[5] M. Shelef, Chem. Rev. 95 (1995) 209.
[6] Y.B. Traa and J. Weitkamp, Micro. Meso. Mater. 30 (1999) 3.
[7] J.N. Armor, Catal. Today 26 (1995) 99.
[8] C.C. Chao and J.H. Lunsford, J. Am. Chem. Soc. 93 (1971) 6794.
[9] O. Monticelli, R. Loenders, P.A. Jacobs and J.A. Martens, Appl. Catal. B 21 (1999) 215.
[10] C. Sedlmair, B. Gil, K. Seshan, A. Jentys and J.A. Lercher, Phys. Chem. Chem. Phys. 5 (2003) 1897.
[11] J. Szanyi, J.H. Kwak, R.A. Molinev and C.H.F. Peden, Phys. Chem. Chem. Phys. 5 (2003) 4045.
[12] J. Szanyi, J.H. Kwak and C.H.F. Peden, J. Phys. Chem. B 108 (2004) 3746.
[13] Y.H. Yeom, B. Wen, W.M.H. Sachtler and E. Weitz, J. Phys. Chem. B 108 (2004) 5386.
[14] S.J. Schmieg, B.K. Cho and S.H. Oh, Appl. Catal. B 49 (2004) 113.
[15] G. Li, S.C. Larsen and V.H. Grassian, J. Mol. Catal. A 227 (2005) 25.
[16] W. Song, G. Li, S.C. Larsen and V.H. Grassian, Env. Sci. Technol. 39 (2005) 1214.
[17] M. Ogura, T. Ohsaki and E. Kikuchi, Micro. Meso. Mater. 21 (1998) 533.
[18] A. Shichi, K. Katagi, A. Satsuma and T. Hattori, Appl. Catal. B 24 (2000) 97.
[19] A. Shichi, A. Satsuma and T. Hattori, Appl. Catal. B 30 (2001) 25.
[20] T. Tabata and H. Ohtsuka, Catal. Lett. 48 (1997) 203.
[21] P. Praserthdam, N. Mongkolsiri and P. Kanchanawanichkun, Catal. Comm. 3 (2002) 191.
[22] Q. Li, D. Creaser and J. Sterte, Chem. Mater. 14 (2002) 1319.
[23] G. Li, M. Xu, S.C. Larsen and V.H. Grassian, J. Mol. Catal. A 194 (2003) 169.
[24] P.O. Fritz and J.H. Lunsford, J. Catal. 118 (1989) 85.
[25] S. Khabtou, T. Chevreau and J.C. Lavalley, Micro. Mater. 3 (1994) 133.
[26] M.J. Remy, D. Stanica, G. Poncelet, E.J.P. Feijen, P.J. Grobet, J.A. Martens and P.A. Jacobs, J. Phys. Chem. 100 (1996) 12440.
[27] D.L. Bhering, A. Ramirez-Solis and C.J.A. Mota, J. Phys. Chem. B 107 (2003) 4342.
[28] S. Zheng, H.R. Heydenrych, A. Jentys and J.A. Lercher, J. Phys. Chem. B 106 (2002) 9552.
[29] K.I. Hadjiivanov, Catal. Rev. – Sci. Eng. 42 (2000) 71.
[30] V.H. Grassian, Int. Rev. Phys. Chem. 20 (2001) 467.
[31] K. Hadjiivanov and L. Dimitrov, Micro. Meso. Mater. 27 (1999) 49.
[32] A. Satsuma, T. Enjoji, K. Shimizu, K. Sato, H. Yoshida and T. Hattori, J. Chem. Soc., Faraday Trans. 94 (1998) 301.
[33] K. Hadjiivanov, D. Klissurski, G. Ramis and G. Busca, Appl. Catal. B 7 (1996) 251.
[34] T.E. Hoost, K.A. Laframboise and K. Otto, Appl. Catal. B 7 (1995) 79.
[35] V.H. Grassian, J. Phys. Chem. A 106 (2002) 860.
[36] M. Haneda, Y. Kintaichi, N. Bion and H. Hamada, Appl. Catal. B 42 (2003) 57.
[37] Y. Yu, H. He, Q. Feng, H. Gao and X. Yang, Appl. Catal. B 49 (2004) 159.
[38] M. Haneda, N. Bion, M. Daturi, J. Saussey, J. Lavalley, D. Duprez and H. Hamada, J. Catal. 206 (2002) 114.
[39] Y. Ukisu, S. Sato, A. Abe and K. Yoshida, Appl. Catal. B 2 (1993) 147.
[40.] G.R. Bamwenda, A. Ogata, A. Obuchi, J. Oi, K. Mizuno and J. Shrzypek, Appl. Catal. B 6 (1995) 311.
[41] W. Schiesser, H. Vinek and A. Jentys, Appl. Catal. B 33 (2001) 263.
[42] S. Sumiya, H. He, A. Abe, N. Takezawa and K. Yoshida, J. Chem. Soc. Faraday Trans. 94 (1998) 2217.
[43] J.M. Garcia-Cortes, J. Perez-Ramirez, J.N. Rouzaud, A.R. Vaccaro, M.J. Illan-Gomez and S. Salinas-Martinez, J. Catal. 218 (2003) 111.
[44] G. Martra, R. Ocule, L. Marchese, G. Centi and S. Coluccis, Catal. Today 73 (2002) 83.
[45] H.Y. Chen, T. Voskoboinikov and W.M.H. Sachtler, J. Catal. 186 (1999) 91.